Spectropolarimetry of Fraunhofer lines in local upper solar atmosphere

Z.Q. Qu[1,2], L. Chang[1,2], G.T. Dun[1], X.M. Cheng[1], C. Fang[3], Z.Xu[1], D.Yuan[4], L.H. Deng[1], X.Y. Zhang[1]

1. Yunnan Astronomical Observatories, CAS, Tinwentai road, Kunming, Yunnan 650216, China
2. School of Astronomy and Space Science, University of Chinese Academy of Sciences, Yuquan road, Chaoyang district, Beijing, China
3. School of Astronomy and Space Science, Nanjing University, Hankou Road, Nanjing, Jiangsu, China
4. Institute of Space Science and Applied Technology, Harbin Institute of Technology, Shenzhen, Guangdong, China

ABSTRACT

Spectropolarimetric results of Fraunhofer lines between 516.3nm and 532.6nm are presented in local upper solar chromosphere, transition zone and inner corona below a height of about 0.04 solar radius above the solar limb. The data were acquired on Nov.3, 2013 during a total solar eclipse in Gabon by the prototype Fiber Arrayed Solar Optical Telescope(FASOT). It is found that the polarization amplitudes of the Fraunhofer lines in these layers depend strongly on specific spectral lines. Fraunhofer line at MgI$b_1$518.4nm can have a polarization amplitude up to 0.36% with respective to the continuum polarization level, while the polarizations of some lines like FeI/CrI524.7nm and FeI525.0nm are often under the detection limit 6.0×10^{-4}. The polarizations of the Fraunhofer lines, like the emission lines and the continuum, increase with height as a whole trend. The fractional linear polarization amplitudes of inner F-corona can be close to those of inner E-corona, and in general larger than those of inner K-corona. Rotation of the polarization direction of Fraunhofer line is often accompanied with variations in their polarization amplitudes and profile shapes. It is also judged from these polarimetric properties, along with evidences, that neutral atoms exist in these atmospheric layers. Thus the inner F-corona described here is induced by the neutral atoms, and the entropy of the inner corona evaluated becomes larger than those in the underneath layers due to more microstates found.

As a common knowledge, solar atmosphere is stratified and formed by the photosphere, chromosphere, transition zone and corona as the heliocentric height increases. In this paper, our study is related to its upper atmosphere containing upper chromosphere, transition zone, as well as inner corona. In these layers, the temperatures of most particles continue to increase with height till the middle layers of the inner corona. This leads to a conclusion hitherto that all the particles

coming from the below layers are heated and ionized in the corona(Golub and Pasachoff,1997; Aschwanden,2015). However, such a view will be changed as demonstrated in this paper.

In order to diagnose the physical conditions, visible light irradiated from quiet solar corona is divided into three parts according to their forms in the literature till now(Golub and Pasachoff,1997; Aschwanden,2015). They are respectively continuum part called K-corona mainly yielded by free electrons scattering the photospheric radiation, E-corona shaped by distribution of emission lines attributed to bound-bound transitions in particles, and F-corona, initially discovered by Moore(1934) and Grotrian(1934), formed via scattering or/and diffracting radiation of absorption(Fraunhofer) lines irradiated from solar photosphere by the dust grains distributed mainly in the ellipsoid around the sun(Lamy et al.,2022; Burtovoi et al.,2022), as an extended corona. Such a kind of scattering is called Mie scattering(Lietzow,2023). After efforts of more than forty years, Koutchmy and his collaborators(Koutchmy et al., 1973; Koutchmy et al., 2019) demonstrated that the projective height(elongation) of the Fraunhofer lines can be very low above the solar limb from eclipse observations. On the other hand, by photometry, its connection to zodiacal light was established (Lamy et al., 1992; Boe et al., 2021; Lamy et al., 2022; Burtovoi et al., 2022).

Polarimetry especially Stokes spectropolarimetry can provide the irreplaceable tool to diagnose the physical conditions. In fact, great efforts for polarimetry of the corona especially F-corona and their theoretical predictions as well as interpretations form a history longer than a century, and solar eclipses have been favorite since they provide the clean environments of minimum scattering and stray light via telluric atmosphere, or observations are performed in space out of the earth with the minimum light pollution. These polarimetries were dominantly concerned of large scales beyond a height of three solar radii($3R_{sun}$) above the solar limb around the sun from broad band observations based on filters. Therefore, polarizations of the F-corona in most cases were not directly obtained but indirectly derived from measured total polarization P_{P+K} and calculated P_K induced from distribution of the free electrons, with knowledge of total intensity and K-coronal intensity(Hulst,1950). One of main scientific goals of these polarimetries is to separate the K- and F-components of the corona and then calculate the electron density as a function of distance from the sun, meanwhile the E-corona is often ignored, though it can be present in the broad band observations.

Therefore, the direct polarimetry of the F-corona was very rare. To our knowledge, Ohman(1947) carried out a spectropolarimetry of solar corona with a lowest height to $0.3R_{sun}$(solar radius) above the limb during 1945 July 9 total solar eclipse. Due to the low spectral resolution and poor signal-to-noise ratio, it was hard to recognize even the Fraunhofer lines from the continuum. This led to that his measured F-corona polarization P_F was very uncertain according to their analysis. It gave an extrapolation result of 0.42 at height of $0.13R_{sun}$ and 0.11 at $0.19R_{sun}$ in G-band listed in his Table XIII, and concluded that the polarization of the Fraunhofer lines was smaller than that of

the continuum. Later, Blackwell and Petford(1966) presented their polarimetric results obtained during 1963 July 20 solar eclipse. In their Table I, percent polarizations of the F-corona were derived from 0.19% at height of $9R_{sun}$(solar radius) to 0.65% at height of $15R_{sun}$ when half-width of the filter bandpass of the polarization channel was set to be 11.6nm. And they constructed an outer solar corona model within which the F-corona polarizations ranged from a very small value 0.05% at height of $5R_{sun}$ to 2.84% at height of $40R_{sun}$, while the polarizations of K-corona were modeled from 59.7% to 61.4%. In his paper, Mann(1992) concluded that dust particles close to the sun influence the coronal brightness strongly, and the calculated F-corona polarization ranges from 0.09% at $8R_{sun}$ to 0.84% at $16R_{sun}$, with zero level at $5R_{sun}$ as the boundary condition. Polarization variation with distance from the sun is fitted by a function of $(r/r_0)^{-p}$ ($p = 2.65 - 2.8$) valid till 0.2AU, and r_0 is the distance between the sun and the earth, i.e., 1AU. They demonstrated that a small polarization by circum-solar particles is necessary to fit their brightness observations. From near-sun observations of the F-corona, Howard and his cooperators(2019) found the intensity decease of the F-corona at short elongations without any polarization data, which was thought to be suggestive of the long-sought dust free zone. Based on data acquired during 2019 July 2 total solar eclipse, Boe and his cooperators(2021) presented the color and brightness of the F-corona, and they found that the total brightness of the F-corona higher than theoretically expected in the lower corona, and deduced that the F-corona is slightly polarized. One outstanding feature of the F-corona is pointed out that the relative line intensities among Fraunhofer lines are very close to their photospheric counterparts(Koutchmy et al., 1973; Koutchmy et al., 2019). Recently, Burtovoi et al.(2022) derived the maps of the F-corona via time correlation of total and polarized visible light images obtained from SOHO/LASCO-C2 (Brueckner,1995; Domingo,1995). The derivation was based on a new analysis of the evolution of the total and polarized brightness images. From the intensity contours of their Fig.15, approximately elliptic shapes of the derived F-corona were found.

In fact, the theories were more precedent to the polarimetry. Early in 1879, Schuster(1879) tried to theorize solar coronal polarization due to Rayleigh scattering. He got a conclusion that the linear polarization should increase with distance from solar center if distribution of the scattering particles obeys inverse power of the distance from the sun. In his Tables, the polarization values were listed respectively, derived from different inverse power distribution, and correspondingly a great range of polarization values were obtained. It is noticeable that Schuster did not take into account the limb-darkening. Half century later, Minnaert(1930) studied the polarization of coronal continuum (i.e., K-corona) in 1930 due to scattering of photospheric light by free electrons, assuming that the electron density distribution could be described as a power function r^n of radius r, and he found that the polarization depends slightly on the wavelength, and polarization amplitude at least 16.4% shown in his Table 6 was expected at solar limb from assuming an electron density variation with the distance of r^{-8} from the sun. However, he found that the measured values

were much smaller than these predicted, and assumed that the corona does not only scatter the photospheric light but also there were some other particles emanating radiation of the continuum. More than twenty-five years later, Grotrian(1956) gave the interpretation of the Rayleigh scattering of solar photospheric light by the particles, and tens of percent polarization amplitudes were estimated. The most memorized theory about the polarization in the early stage was given by van de Hulst(1950). He formulated the polarization of the corona, but found his theoretical results of K-corona greater than observed values then, and thus ignorance of F-corona polarization might lead to discrepancies. In his theory, the polarization was wavelength-independent in a narrow band if only Rayleigh scattering was considered. A curve describing variation of the F-corona percentage polarization with elongation was given by Blackwell(1956) from his theoretical calculation. He showed an ignorable value close to solar limb but high percentage polarization of about 15% at elongation 60°, and his actual measurement from an aircraft during a total solar eclipse led to much higher values. For instance, the theoretical prediction was less than one percent at elongation of 5° but his polarimetry resulted in a value of 2.8%, which was used for identification of the zodiacal light as the outer F-corona. Very recently, since the brightness of F-corona in the low corona is measured to be more intense than expected by assuming unpolarized F-corona, Boe and his cooperators(2021) are doubting the assumption. A method for separating K-corona and F-corona is proposed by Burtovoi et al.(2022) via acceptance of less than 0.06% linear polarization amplitudes of the F-corona below $6R_{Sun}$, calculated by Blackwell and Petford(1966). Nevertheless, these theoretical predictions differed considerably due to their different assumptions and many inconsistencies among the polarimetric results and the theoretical calculations lead to chaos in this literature.

1. Observation and Data reduction

The spectropolarimetric data were obtained during 2013 total solar eclipse observation by the prototype Fiber Arrayed Solar Optical Telescope(FASOT)(Qu, 2011; Qu et al.,2014), observed at Bifoun of Gabon on Nov.3, 2013. The observation aimed at real time spectroimaging polarimetry within a band from 516.3nm to 532.6nm containing multiple spectral lines(Qu et al.,2017; Qu et al.,2022), and data used here are only a small part of the dataset. The instrument and some observational details were introduced in the last two cited papers, but necessary details are described again below in order to make a brief and clear picture about the spectral images shown respectively in top panels of following Figures 2-6. In our last two papers, we presented respectively spectroimaging polarimetry of the green coronal line(Qu et al.,2017)(referred to Paper I hereafter), and spectropolarimetry of all the emission lines observed(Qu et al,2022)(referred to Paper II hereafter), but remained polarimetric demodulation and analysis of the Fraunhofer lines and continuum observed in the upper solar atmosphere in this paper due to its abundant content.

The approximate positions of observational field of views(FOVs) of sample data documented with SE196-2, SE196-4, SE204-3 and SE205-1 are indicated by the white squares (not to scale) artificially superposed on corresponding eclipse monitoring images respectively shown in three panels of Figure 1, where the bright sickles were white-light images of the sun blocked by the moon in process of approaching the second contact. Each of the two FASOT integral field unit(IFU) head structures defining the same field of view(FOV) is formed by 5×5 microlens array receiving radiation from spatially resolved points in the sun, coupled with fiber array behind one by one and coded in the bottom right panel of Fig.1. Each spatial volume covers 2×2 arcseconds or approximately 1500km×1500km cross-section transversally in the sky plane. The fibers forming the array in the IFU head are re-weaved into one pseudo slit dispersed by a spectrograph. The spectral images on top panels of Figures 2-6 are obtained after dispersion of the fifty beams coming out of the fifty fibers contained in the slit. It is worthy to note that in order to carry out the accurate linear polarimetry, the light beam originated from each of the solar spatial volume is split by the polarizing beam splitter into two beams with opposite polarization states denoted by $'a'$ and $'b'$ in spectral images on top panels of Figs.2-6, received by the pair of IFU. Thus there are 50 rather than 25 spectra as relatively bright horizontal strips in each top panel of these figures. The intensity and fractional linear polarization are demodulated from each couple of fibers respectively. The two spectra of each couple are arranged symmetrically about the central dark horizontal belt between the two twenty-fifth couple spectra. For instance, the two beams of the first couple($1a$ and $1b$) are placed respectively on the bottom and the top rows, and the other couples move to the cental line orderly, as illustrated in the right columns of the top panels of these figures. The intensities of $'a'$ and $'b'$ of one couple can be described by $1/2(I + Q)$ and $1/2(I - Q)$ respectively multiplied by the extinction factors caused by the time-dependent telluric atmospheric seeing and different light paths within the telescope(see Papers I and II). A geographic direction indicator is also plotted on the left side in the bottom right panel of Fig.1 together, and the positive linear polarization Stokes Q is defined along the North-South orientation.

The polarimetric demodulation technique was described in Paper I and then improved in Paper II, and again we adopted the method described by Eq.(3) in Paper II. However, unlike data reduction of emission lines in Paper II, where most of the polarimetric demodulations were executed for each resolved spatial point with an intensity threshold above the continuum level. The demodulation of the Fraunhofer lines in the upper solar atmosphere will not become feasible especially at the line centers with the least residual intensities for each resolved spatial point, due to the noise fluctuation typically of tens of readout photon counts leading to polarimetric noise level of 6.0×10^{-3}, a value greater than all these demodulation signals in the following. Therefore a spatial binning over rows of the FOV(referred to the diagram in the bottom right panel of Fig.1) becomes necessary to obtain the reliable polarimetric results without demodulation threshold. This leads to reduction of the spatial resolution but enhancement of the polarimetric signal-to-noise ratio, and

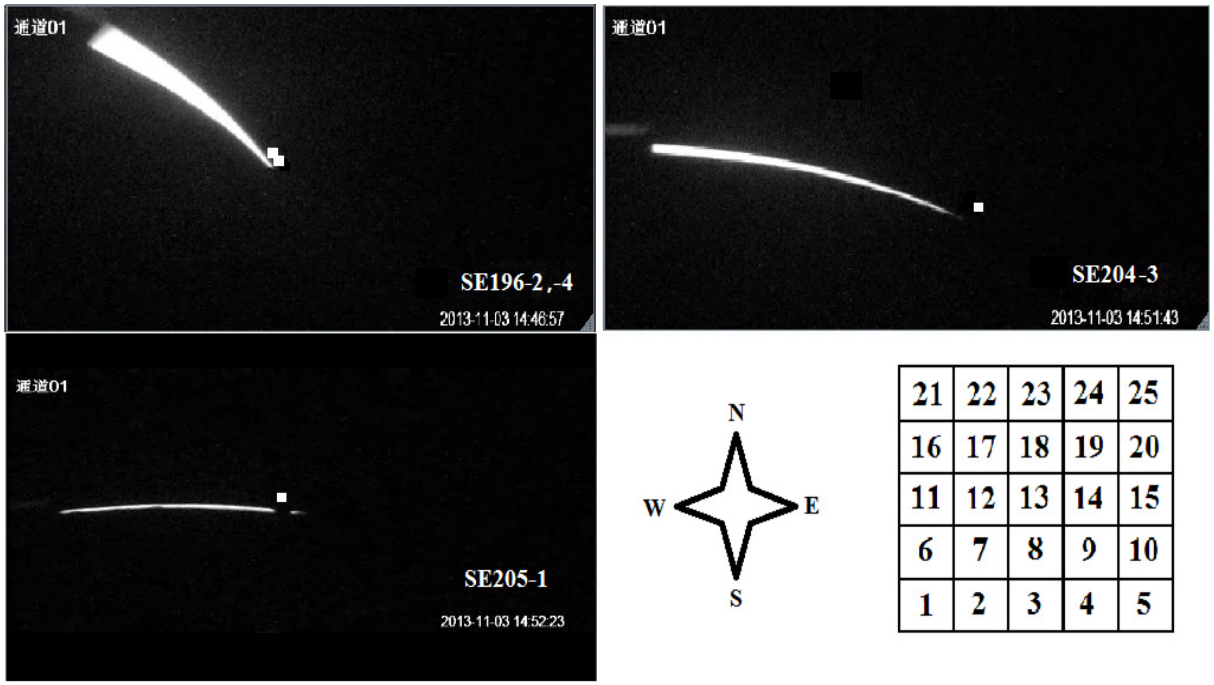

Fig. 1.— Approximate locations of fields of view (FOVs) of the polarimetric data samples analyzed in the text, directional indicator and alignment configuration of the lenslet-coupled fiber array as the head of Integral Field Unit (IFU) of the prototype FASOT. Top two and bottom-left panels: bright sickles were solar crescents formed by lunar occultation in process of the eclipse. Artificial white squares corresponding to the bottom-right square icon superposed in these monitoring images, not to scale, indicate approximately estimated positions of FOVs. The monitoring images of SE196-2 and SE196-4 are combined on the top left panel, that of SE204-3 is plotted in the top right panel, and that of SE205-1 in the bottom left panel. The location of SE196-2 is a little higher than SE196-4. Bottom right panel: the directional indicator placed on the left, and on the right is the alignment configuration of 5×5 spatial points of the FOVs indicated as the white squares in the other panels of this figure.

reliable polarization information of the continuum spectra becomes also available simultaneously.

The Stokes polarimetric result of the quiet sun region at the solar disk center before the eclipse can be used to provide a standard photospheric Fraunhofer lines. Otherwise, in order to detect the effect of above-mentioned binning and check the accuracy of the polarimetry, we demodulate the photospheric data named SE90-1 acquired at the disk center in the quiet sun region with a small fractional aperture of the telescope used before the eclipse. Three sets of demodulated intensity I and percent linear polarization represented by Stokes Q/I profiles are depicted in Fig.2 for specifying the binning effect. The intensity is in unit of the readout photon counts(cts) of detector throughout the paper.

Top panel of Fig.2 provides the raw spectral image of the photospheric Fraunhofer lines within the observational band from 516.3nm to 532.6nm. According to the spatial symmetry, the polarization here should be zero. Since we have enough photon budget in this photospheric case, a sample demodulation of the second resolved spatial point P2 without binning is displayed in the second and third panels(counted from top to bottom and hereafter). The fractional polarization noise does not exceed 1.0×10^{-3} with respective to(wrt) the continuum level. Then we perform the binning over the three lower rows of the FOV, i.e., from point one to point fifteen(indicated by P1-P15 and similar in the following), shown in the fourth and fifth panels. It is markable that the polarimetric noise is reduced to be below 3.0×10^{-4} wrt the continuum polarization level. Finally, we present the result after binning P16-P25. The polarimetric noise level is smaller than the single point P2 but greater than the binning P1-P15 which contains more spatial points. However, since the scattering and stray light was greatly depressed, the polarimetric accuracies will be increased correspondingly for these data acquired close to the totality. It is noteworthy that the polarization of the quiet sun region at the disk center is used for polarization zero calibration(Bianda,1998) as pointed out in Paper II.

2. Spectropolarimetric results of Fraunhofer lines during the eclipse

In this section, we present four polarimetric cases respectively in an order according to their acquisition times. Two samples show Fraunhofer lines coexisting with emission ones in the same FOVs but without any coronal line, and the other two are cases of Fraunhofer lines present with the emission lines including the green coronal line.

As pointed out previously, the residual intensity of a Fraunhofer line of single spatially resolved point is too faint for us to get enough polarimetric signal-to-noise ratio, we have to carry out divisions of the FOV via the spatial binning to promote the ratio. The division is classified into two kinds in this paper. One is executed in such a way that the binning is performed over respectively

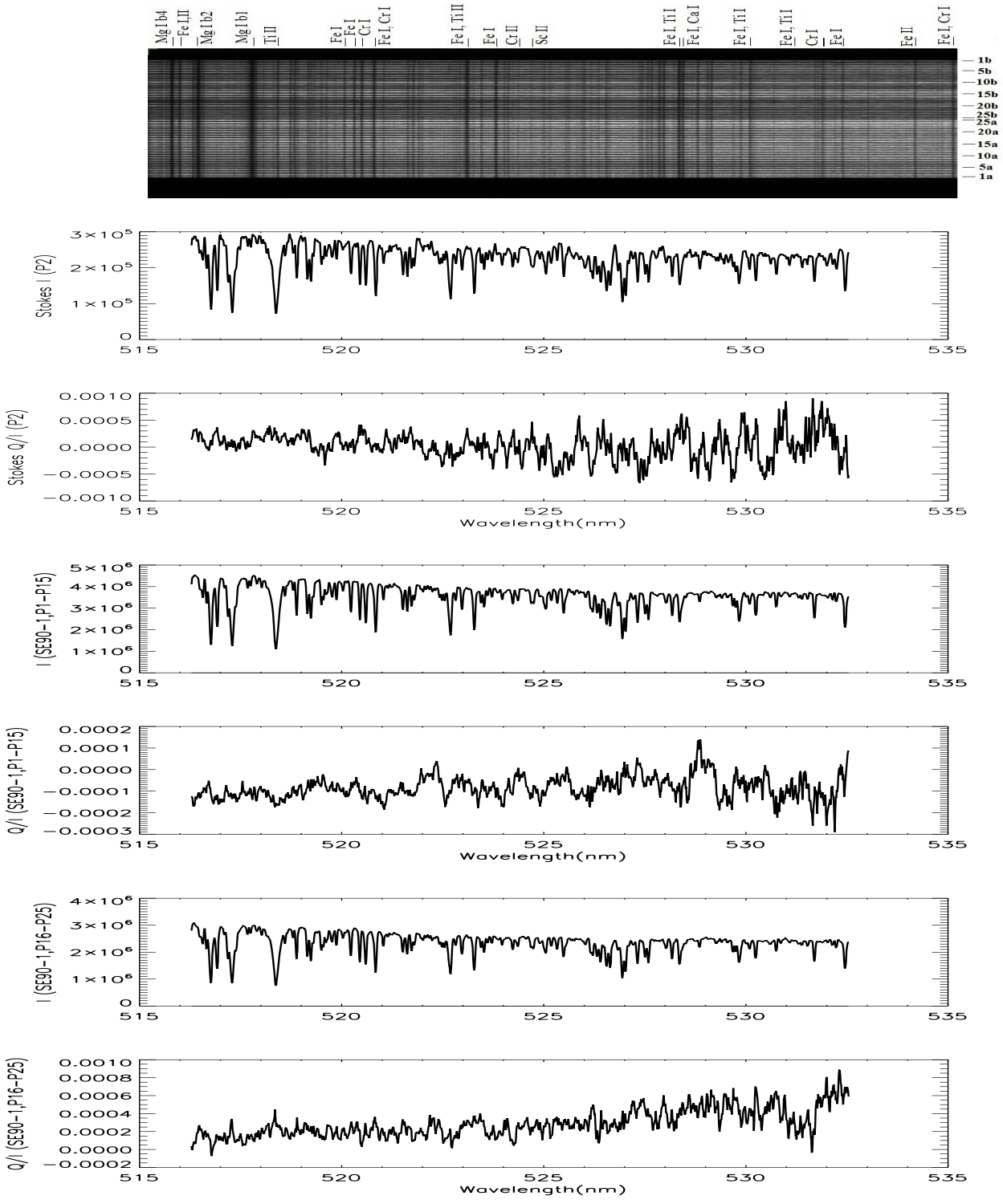

Fig. 2.— Sample polarimetric results acquired at the disk center before the eclipse. The demodulated intensity and the fractional linear polarization Q/I profiles without and with binning performances are plotted below the raw spectral image to show the enhancement of the polarimetric accuracy with the spatial binning. The symbols above the top image indicate the line producers with their ionization state, and the numbers attached with letters 'a' and 'b' in the rightmost column reflect ordinary and extraordinary light beams originated from the incident volume array described in the bottom-right panel of Fig1. The intensity I is obtained via adding the dual beams with the same numbers, and Q/I is demodulated also from the dual beams via a technique called Reduced Polarimetric Optical Switching(RPOS), and hereafter in the figures.

the lower three rows and then the upper two rows of the FOV. The other is accomplished respectively over the lower two rows and then the upper three rows according to the need(cf. bottom-right panel of Fig.1). Otherwise, binning over all these spatial points in the FOV is performed so that we can see further polarimetric result over a larger spatial volume and furthermore how spatial integration influences the polarimetric consequences. Finally, it is valuable to bear in mind that intensity of one spatial point is an integration along line-of-sight of radiative sources with different heliocentric heights, and polarization amplitudes of spectral lines described below are generally referred to be with respect to(wrt) their adjacent continuum polarization level.

2.1. Spectropolarimetric results of Fraunhofer lines without the coronal line

The Fraunhofer lines are dominantly originated from the photosphere in appearance of absorption under the background of the thermal pool formed by the frequent particle collisions(Mihalas,1969), and the absorption dominates the emission. However, they can be also produced in local upper regions where the collision plays still an important role or observed via Rayleigh scattering. Whether these Fraunhofer lines can survive in the inner corona is just what we want to investigate. In this subsection, we select two cases named SE196-2 and SE196-4 within one set of data SE196, which contains six frames acquired with an exposure time of three seconds for each frame, about four and half minutes before the totality, when the bright solar crescent formed by lunar occultation was still prominent as seen from the top left panel of Fig.1, where the FOV of SE196-4 locates a little lower than SE196-2 above the local solar limb. In fact, there are more than twenty frames acquired with abundant spatial distribution patterns of the Fraunhofer and emission lines together without the coronal line present in the same FOVs. The distribution patterns of the Fraunhofer lines in the FOVs of these two selected samples can be representatives. They are regarded to be in upper chromosphere and extended into the transition zone judged from their presence above their chromospheric emission counterparts such as neutral magnesium triplet(MgI $b_1 : 518.4nm, b_2 : 517.3nm$ and $b_4 : 516.7nm$), and the transition zone emission lines represented by once ionized iron emission lines, such as FeII531.7nm. It is noteworthy that no regularly geometrical boundaries between the corona and transition zone, or even between the transition zone and chromosphere, as a common sense in the literature. Therefore the emission lines can extend to different heights in different regions, the identification of the forming locations of the Fraunhofer lines concerned depends on their distribution compared with these emission lines.

2.1.1. SE196-2

The first case named SE196-2 is depicted in Fig.3. The raw spectral image is shown in the top panel. It is seen that most Fraunhofer line appearances can be seen in these points above those yielding their emission line counterparts, but the transformation from line emission to depression depends on spectral lines at different spatial points. This can be ascribed to their different emission, absorption and scattering along the line-of-sight, and differs from the scenario caused purely by dust scattering. Especially, there are few weak Fraunhofer lines keeping their absorption appearance in almost the whole FOV, such as CaI526.0nm, FeI521.6nm, CrI/FeI/FeII527.3nm, CrI529.8nm and CrI530.1nm.

The second and third panels(counted from the top to the bottom and hereafter) present respectively the intensity I and corresponding fractional linear polarization Q/I profiles of a spatial domain covering the three lower rows of the FOV(referred to bottom right panel of Fig.1). The Fraunhofer lines are hard to be seen in the second panel, due to depression by the emission lines via linear intensity contrast. But this is not the case for their Q/I profiles. Besides the prominent polarizations at most of the strong emission lines, the very weak Fraunhofer lines of mixed CrI/FeI/FeII527.3nm and CrI529.8nm are polarized with Q/I amplitudes comparable to those of the emission lines with largest Q/I polarizations. Some of other Fraunhofer lines like these at 521.3nm, 523.2nm, 527.9nm and 531.5nm gain distinguishable Q/I amplitudes comparable to these of some medium strong emission lines. But polarizations of most of the Fraunhofer lines merge still in noise.

When the spatial binning is performed over the two higher layers(P16-P25), shown in the fourth and fifth panels, the Fraunhofer lines become dominant now, and their relative line depths are changed from the photospheric counterparts shown in Fig.2. Polarimetrically, FeI/CrI532.4nm line attains the greatest amplitude of about 0.32% with respective to(wrt) the local continuum level 0.28%. The magnesium triplet and these lines around respectively 526.6nm, 527.0nm, 529.0nm, while lines at 529.8nm and 531.8nm obtain considerable polarizations, but many of the Fraunhofer lines including some strong ones remain to own no detectable polarization signals.

After the whole FOV binning is performed as shown in the two bottom panels, it is evident that both the I and Q/I profiles look much closer to those in the lower layers. This is understandable since that much greater number of photons and polarized photons are contributed there. However, the contribution of these polarizations below the continuum level from the higher layers are observable. For instance, the large negative amplitude of the 532.4nm line is more ascribed to the upper layers. And the most prominent positive Q/I value locates at 527.6nm in the lower layers but now transfers to MgI b_1 line. It becomes evident that the polarimetric noise level decreases, as more easily witnessed in the subband with wavelengths larger than 532.0nm.

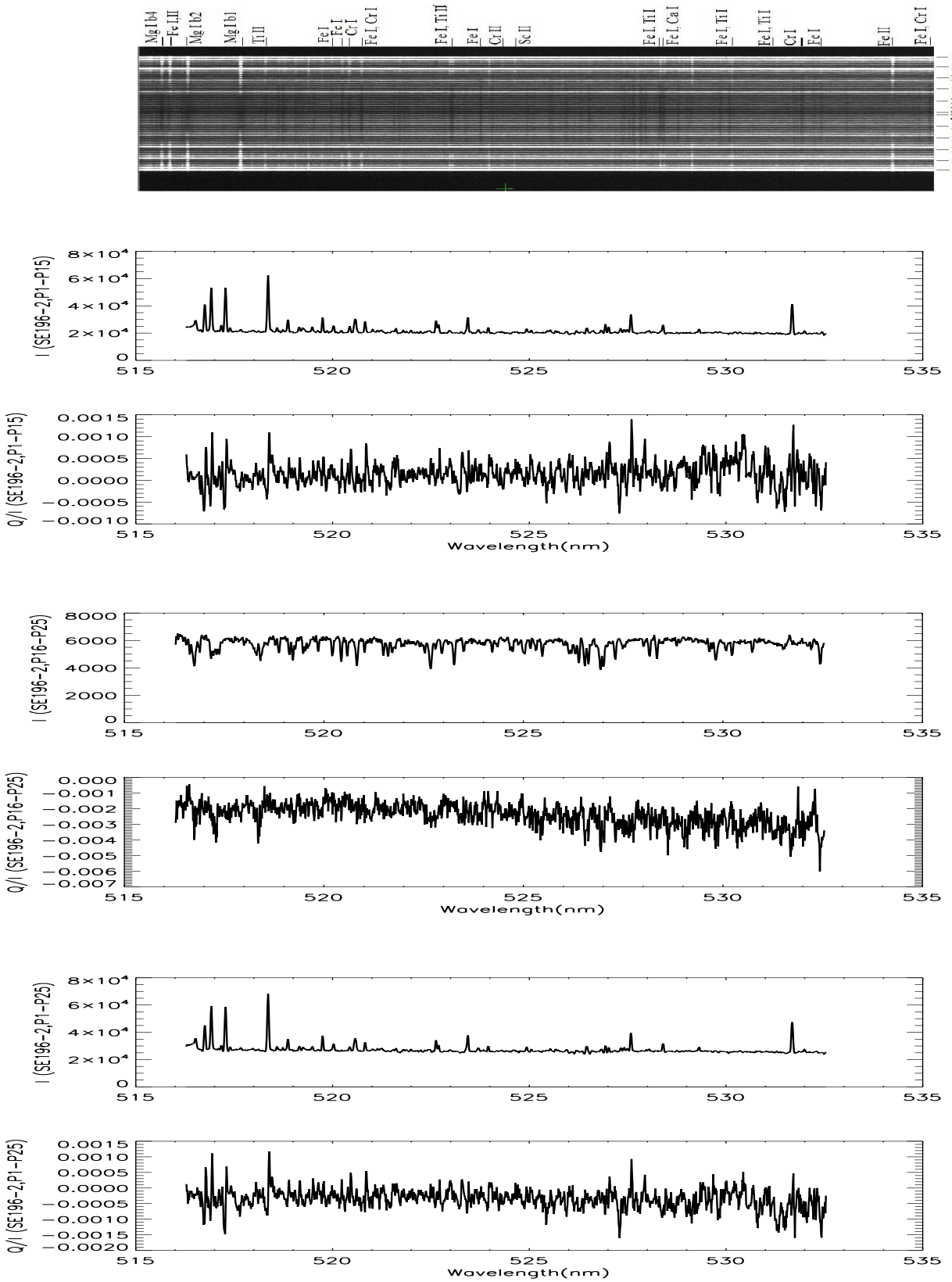

Fig. 3.— SE196-2. Top panel: the raw spectral image. Lower panels: the intensity I and fractional linear polarization Q/I profiles obtained from polarization demodulation after spatial binning over P1-P15(cf. bottom panel of Fig.1), P16-P25 and the whole(P1-P25) of the FOV respectively.

Therefore, it becomes evident that the polarizations of the Fraunhofer lines, like their emission counterparts also described in Paper II, depend on specific lines. On the other hand, as a whole trend, the polarization amplitudes of these lines increase when they are transformed from the emission lines to the Fraunhofer ones with detectable polarization. In fact, the polarization plane rotation can be seen in not all but many lines that in the lower layers there are positive polarizations in the red wings and negative ones in the blue wings but in the higher domain, the polarization becomes dominantly negative.

2.1.2. SE196-4

The second case is SE196-4 with its FOV lower than SE196-2. It shows evidently another distribution pattern of alternative domination of the emission and absorption in different lines from Fig.4. Most lines own emission appearance in the lowest rows of the FOV but some lines turn to be Fraunhofer lines in higher layers like FeI/NiI519.2nm, FeI520.2nm, FeI/CrI520.4nm, CrI520.6nm and CrI/FeI520.8nm, while more lines especially the strong ones keep a form of emission in the whole FOV, such as the quartet(chromospheric magnesium triplet and the mixed FeI/FeII516.9nm, and hereafter), transition zone lines of FeII531.7nm. However, most of these emission lines are not of pure emission but with absorption feature in their far wings in detail. On the other hand, some weak Fraunhofer lines like FeI526.3nm, CaI526.6nm and CrI/FeI532.4nm maintain their absorption form in the whole FOV, which implies their photospheric origin. It is seen that the quartet is the strongest, then followed by the two mixed emission FeII531.7nm lines. The relative intensities among these Fraunhofer lines in the higher layers(cf. the fourth panel of Fig.4) are not consistent with those of the photosphere. For instance, CaI/FeI527.0nm becomes much weaker than those in Fig.2 compared with its surrounding lines.

The second and third panels of Fig.4 show respectively the intensity I and fractional linear polarization Q/I of a spatial domain covering the three lower rows of the FOV(referred to bottom right panel of Fig.1), i.e., from the first volume to the fifteenth one(P1-P15). It is very hard to see the Fraunhofer lines, because that they are greatly depressed by the emission lines via contrast. However, it can be seen that the very weak Fraunhofer lines of mixed CrI/FeI/FeII527.3nm and FeI/CrI/NdII529.4nm are polarized with prominent Q/I amplitudes. And groups of lines around 517.6nm, 521.4nm, 523.2nm, 525.5nm, 529.2nm and 531.4nm containing very weak Fraunhofer lines yield evident Q/I valleys. It is valuable to note FeI/CrI532.4nm line with a very weak emission appearance, its polarization is prominent. Its polarization turns to be stronger in the higher elongations where it turns to be a Fraunhofer line. High signal-to-noise ratios of polarizations of the quartet and the transition zone emission lines can be seen. Some of them have Q/I amplitudes close to 0.10%. These Q/I profiles of the quartet and other lines are approximately antisymmetric

about their line centers. In detail, the polarizations in the blue wings of these lines are negative(along East-West direction) and those in the red wings positive(along North-South direction). It is easily deduced that if one carries integration along dispersion over the spectral lines individually, the integrated polarization amplitudes will become much weaker or even canceled out. This specifies the importance of spectral resolution in polarimetry. It is also noted that this kind of Q/I profile is not shared by some other lines such as FeII531.7nm that has an outstanding single peak in its Q/I profile. Finally, some Fraunhofer lines have no detectable polarization like 522.3nm, 524.2nm, 524.8nm, 526.3nm and 526.6nm. Therefore, the Q/I profile configuration depends on spectral lines and space.

The situation changes when the binning is performed over the higher layers, seen from the fourth and fifth panels of Fig.4. The Fraunhofer lines become a little more easily distinguishable now. More Fraunhofer lines are found without detectable polarizations, like lines respectively at 519.2nm, 520.2nm, 523.0nm, 523.6nm, 524.2nm, 528.2nm, 528.4nm, 529.7nm, 529.0nm, 530.7nm and 531.5nm. The style of Q/I profile turns to be simpler with a negative single valley or a single peak. The polarimetry becomes more noisy with RMS 6.30×10^{-4} greater than 1.72×10^{-4} of the former binning. The amplitudes become larger for these strongly polarized lines like the magnesium emission triplet and the Fraunhofer line FeI/CaI527.0nm, while the mixed FeI/CrI/NdII lines at 529.4nm become too weak to be detected. Another Fraunhofer line CrI/FeI/FeII527.3nm can be seen from the I profile, its polarization looks not so prominent but actually larger than that in the lower layers. On the contrary, the Fraunhofer FeI521.7nm and FeI/CrI532.4nm lines become more remarkably polarized. It is evident that in general, the polarization amplitudes of the Fraunhofer lines become larger than their emission counterparts in the lower layers for more lines, no critical variation in polarization is found compared with those pure Fraunhofer lines covering the whole FOV, or only partial FOV.

Now, let us see the result after the whole FOV binning shown in the two bottom panels. The Q/I profile looks again closer to that in the lower layers. But the amplitudes of negative lobes standing below the continuum polarization level of Q/I profiles of the quartet are enhanced due to the contribution from the higher layers, and number of lines with pure positive Q/I amplitudes in the lower layers is reduced such as FeI/TiII522.7nm line. However, because that its polarization directions are the same in the two divided domains, the polarization amplitudes of FeI/CrI527.3nm line becomes greater than in the lower layers. Finally, it is easily concluded that different spatial resolutions lead to different polarimetric results according to the binning schemes. This indicates that the lines are not homogeneously but variably polarized in space.

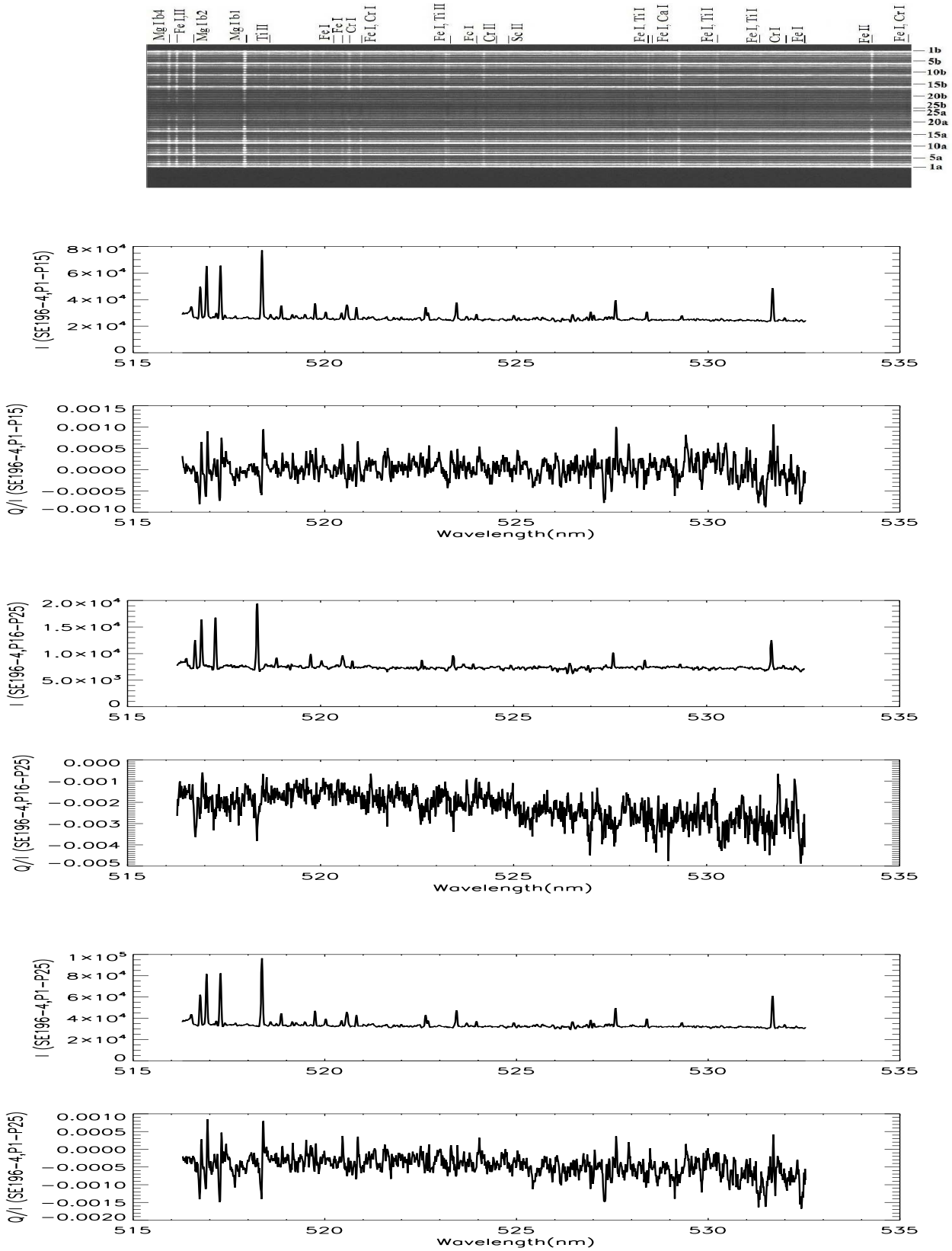

Fig. 4.— SE196-4. Top panel: the raw spectral image. Lower panels: the intensity I and fractional linear polarization Q/I profiles obtained from polarization demodulation after spatial binning over point one to point fifteen(P1-P15), P16-P25 and all the points(P1-P25) of the FOV respectively.

2.2. Spectropolarimetric results of Fraunhofer lines with the coronal line

Spectropolarimetry of Fraunhofer lines in this section differs from that of the above-mentioned one only in a way that they share the same line-of-sight space projected into the sky plane with the green coronal line, and so do other emission lines. Although it is difficult to precisely locate these spatial points yielding Fraunhofer lines due to the projective effect, they can be regarded definitely as parts of the F-corona when they are formed above the elongation where the net green coronal line intensity above the continuum becomes the strongest. The strongest net intensities of the green coronal line above the continuum locate at P11, P2, P18, P4 and P5 at columns of the FOV from the left to the right for SE204-3. For SE205-1, these points with greatest intensities in these columns of the FOV locates at P11, P2, P3, P4 and P5. Radiation from above these elongations can be definitely judged in the corona.

2.2.1. SE204-3

The spectral image plotted on top panel of Fig.5 shows SE204-3 case as one kind distribution of the Fraunhofer lines, where only several lines have appearance of emission in the lower elongations but change to absorption one in the larger heights. The FOV of SE204-3 locates at an estimated height of $0.04R_{sun}$(cf Fig.1), higher than SE205-1. Although it is found that the Fraunhofer lines keep roughly their relative intensities as those of the photosphere in some wavelength interval, but many exceptions are found. For instance, photospheric lines of the quartet especially MgI516.7nm and FeI/FeII516.9nm, 518.7nm, 518.8nm, 519.1nm, 520.5nm, CrI/CrII/FeI527.5nm and FeI/CrI532.4nm become much weaker compared with their neighboring lines. The transition zone lines at 531.7nm and the mixed FeII/FeI/NiI519.7nm always take a form of emission as the green coronal line, but their intensities become weak with height much more greatly than the latter. At P1, only the green coronal line, FeII531.7nm and FeII/FeI/NiI519.7nm take a pure emission appearance, while MgIb_4 owns a pure absorption profile and keeps it in the whole FOV. It is interesting that the MgI$b_{1,2}$ have an emission feature in the line cores and absorption character in line wings. Moving horizontally along the first row to the right(cf. Fig.1), the emission feature becomes stronger and stronger and the absorption weaker and weaker till P5. On the second row, the emission decays correspondingly. This shows how the emission appearance emerges and disappears for those lines with both the partial emission and absorption features.

Since most of these emission lines are confined in the lowest two rows of the FOV, we perform the first polarimetric demodulation after the spatial binning over these two rows, i.e., P1-P10. The second and third panels of Fig.5 provide the corresponding integrated intensity I and its corresponding fractional linear polarization Q/I profiles. At first glance, it is noticed that the polariza-

tion level of the continuum becomes now evidently negative. Q/I profiles of these emission lines in the short wavelength band are different from those of SE196-2. The Q/I amplitude of magnesium b_2 line becomes weaker and the blue wing of its Q/I profile is greatly broadened. The emerged green coronal line gains a Q/I amplitude of only about 0.07%. Although the FeII531.7nm lines have intensity larger than the green coronal line, its polarization is undetectable, unlike the two previous cases. Meanwhile, its neighboring weak Fraunhofer line FeI531.5nm attains an impressive polarization as a contrast. Another emission line FeII/FeI/NiI519.7nm has neither detectable polarization in both the lower and higher layers.

Now, let us focus on the other Fraunhofer lines. Outstanding phenomenon occurs that there are at least four appreciable polarization valleys appearing respectively around 517.7nm, 518.2nm, 525.5nm, 526.0nm and 530.2nm, containing many weak Fraunhofer lines and including their adjacent continuum. Such kind of polarization valleys can be also found in SE196-4 in the lower layers around 523.0nm and 531.5nm. It is noticeable that this phenomenon is also found in the second solar spectrum(Gandofer,2000), say, around 396.0nm, 428.0nm, 435.2nm, 517.2nm, 518.4nm 589.5nm. The FeI/CrI532.4nm is only one Fraunhofer line whose Q/I amplitude surpasses 0.1% wrt the adjacent continuum level. The strong mixed FeI/CrI lines at 520.4nm and 520.8nm are polarized with considerable amplitudes, and so do the weak lines at FeII/FeI/CrI526.6nm, FeI/CaI527.0nm and FeI531.5nm. However, Q/I profiles of the former two lines gain profiles of approximately antisymmetry. And so do the magnesium b_4 absorption line, FeI523.3nm, CrI527.2nm and FeI/NiI528.2nm. Therefore, such a kind of profile feature is not owned only by the emission lines. On the other hand, some strong Fraunhofer lines such as FeI520.2nm, 522.7nm, 525.0nm, 526.3nm, and FeI/CrI524.7nm have no detectable polarizations. On the whole, different lines behave distinguishably according to the polarimetric results, but no critical difference of profile configuration is found between the emission and Fraunhofer ones. Like the previous cases, the percent polarization has nothing to do with the line intensity.

The intensity and fractional linear polarization profiles obtained after binning over the three upper rows are depicted in Fig.5, along with the spectral image on the top. As before, fewer Fraunhofer lines are detected to be polarized, but the polarization amplitudes remarkably increase in these higher layers. The Q/I profiles depicted in the fifth panel of Fig.5 look similar to those derived from the former cases in the short wavelength domain. It is clear that the detectable polarization amplitudes increase in SE204-3 compared to these two above-mentioned cases. A great amplitude of about 0.36% is gained by the MgIb_1 line wrt the continuum level while in SE194-2 and SE196-4 it is less than 0.25%. The strong Fraunhofer line FeI/TiII522.7nm obtains prominent polarization, but such scenario can be found neither in the lower layers nor in the two previous cases. On the contrary, it is noteworthy that the Fraunhofer FeI/FeII516.9nm line becomes much weaker, and so is their polarization. This is very different from its emission counterparts in the lower layers as an exception of polarization amplitude enhancement with height. The polarization

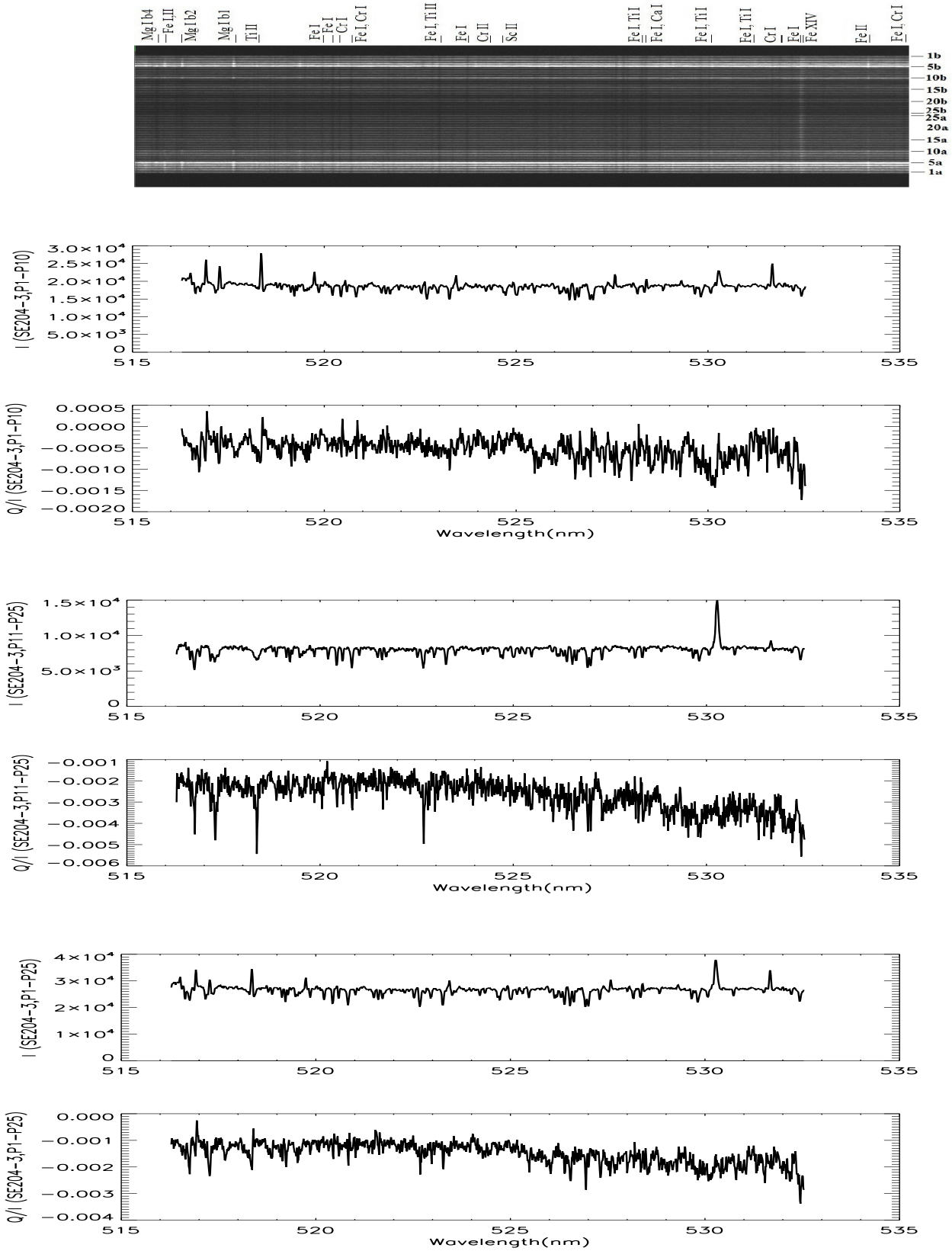

Fig. 5.— SE204-3. Top panel: the raw spectral image. Lower panels: the intensity I and fractional linear polarization Q/I profiles obtained from the polarization demodulation after spatial binning P1-P10, P11-P25 and all the volumes(P1-P25) of the FOV respectively. The green coronal line is the broadest line at 530.3nm. Note that the polarizations averaged over the upper layers(P11-P25) are given of F-corona, E-corona and K-corona.

of the green coronal line is considerably polarized in the lower region but seems to be under the detection here. This is due to the rotation of the polarization direction within these points, as also seen in Paper I and Paper II, and then canceling out by the spatial integration. It is noteworthy that the polarimetric results of the Fraunhofer lines and the continuum in these layers tell us that polarization amplitudes of F-corona are definitely larger than those of K-corona.

In summary, the transformation of the emission line to the Fraunhofer ones seems to change their Q/I profiles and enhance their amplitudes for some strong lines like the magnesium triplet, but opposite change happens for other lines such as FeI/FeII516.9nm which has no detectable polarization in the greater heights, and no change occurs for other lines like FeII523.4nm and FeI/TiI528.3nm without polarization signals out of the noise level in both the domains. For these lines keeping their Fraunhofer profiles in the whole FOV, some lines attain polarization detected in the lower region but lose it in the higher like FeI523.3nm. For strong Fraunhofer lines like FeI522.7nm, it gains visible polarization in the higher layers rather than in the lower one. For those Fraunhofer lines at 520.4nm and 520.8nm, their Q/I amplitudes stand above the continuum level in the lower region but with greater amplitudes below the continuum in the higher one. Finally, for these green coronal line and transition zone line FeII531.7nm, they keep their emission appearance in the entire FOV. The coronal line is more polarized in the lower heights and the transition zone line is not found to be polarized in the lower layers but it seems to have a little Q/I amplitude in the upper ones. On the whole, the variation with height is complicated, rather than consistent.

The Q/I profile shapes obtained after binning over all the spatial points, plotted in the bottom panel, becomes evidently different from the counterparts of the two previous cases, not only at the quartet, but also in the long wavelength domain. For instance, Q/I profile of MgIb_2 line has only a valley here but owns a peak else in the other two cases. On the whole, the negative amplitudes below the continuum level dominate in the present case, but these above the continuum one become fainter. The mixed FeI/CrI/TiI532.4nm lines have the greatest Q/I amplitude of almost 0.20% wrt the continuum level due to absence of cancelation of opposite polarizations, once again greater than in the above-mentioned cases. On the contrary, the fractional linear polarization of the green coronal line FeXIV530.3nm is shown to be almost under detection after the binning over the whole FOV, again due to cancelations of Q/I amplitudes with opposite polarization directions in the binned space. On the other hand, a group of Fraunhofer lines around 527.0nm attains impressive polarizations. The averaged continuum polarization amplitudes reach about -0.12% at the shortest wavelength to -0.17% at the longest wavelength.

2.2.2. SE205-1

The last case is SE205-1, acquired with an exposure time of five and half seconds, only nearly eleven seconds before the second contact. The integrated I and Q/I profiles are depicted just below the top panel of Fig.6. The Fraunhofer lines exist in a way similar to SE196-4. For instance, lines at 521.6nm, 521.8nm, 522.5nm and 522.7nm are hardly recognizable in the lower layers. It is not difficult to find that the relative intensities among the remanent strong Fraunhofer lines in the upper domain become close to each other, as evidenced from I profiles plotted in the fourth panel, very different from the spectra acquired in the quiet sun region before the eclipse(cf. top panel of Fig.2). It is valuable to note from the bottom left panel of Fig.1 that just in this case, the negative Q polarization along the East-West becomes approximately tangential to the local limb now.

It is evident that the linear polarization profiles obtained after binning over the two lower rows in the FOV are not so similar to those of SE196-2 or SE196-4 shown in Figs.3-4, but closer to that of SE204-3 though its intensity profiles are easily distinguishable from those of SE204-3 but closer to the previous cases. Now, the continuum polarization is negative throughout the band and vary from about 0.07% in the shortest wavelength to 0.13% in the longest. Contrast to many strong emission lines, it is remarkable that the fractional linear polarizations of most of the Fraunhofer lines integrated over P1-P10 are not well off the continuum, like the Fraunhofer lines themselves in the spectral intensity I image. However, exceptions are present. The large polarization valleys made by Fraunhofer lines respectively around 518.0nm, 526.9nm and 530.0nm can be still be seen. At about FeI/CrI532.4nm, the fractional polarization amplitude wrt the continuum approaches a value of 0.2%. Other Fraunhofer lines like FeI525.0nm line, their percent linear polarizations can hardly be distinguishable from the continuum one, while RMS of the polarimetric noise level reads as 3.34×10^{-4}. In this case, the polarization of the coronal line is very prominent. Its Q/I amplitude stands up in the large valleys around it.

Moving to the upper layers formed by P11 to P25 in the FOV, the situation becomes changed. Both of those Fraunhofer lines themselves and their detectable polarizations become evidently visible with considerable fractional linear polarization signals. Polarization of the Fraunhofer FeI522.7nm line in the upper layers becomes again the most prominent, like the corresponding situation in upper layers of SE204-3 but different from the other two cases, with an amplitude close to 0.30% as that of MgIb_2. Those Q/I amplitudes of the Fraunhofer FeI/CrI520.4nm and 520.8nm are also remarkable, comparable to the weak emission line MgIb_4, even stronger than the green coronal line which now becomes the strongest emission line and its polarization stands still within the center of the polarization valley, while it is much weaker in the lower layers compared with other strong emission lines. The strong emission line FeI/FeII516.9nm has Q/I polarization less prominent than its neighbor MgIb_4 line. Another outstanding polarization is occupied by emission ScII/CrI 531.8nm line but rather than FeI/FeII531.7nm. And once again the Fraunhofer

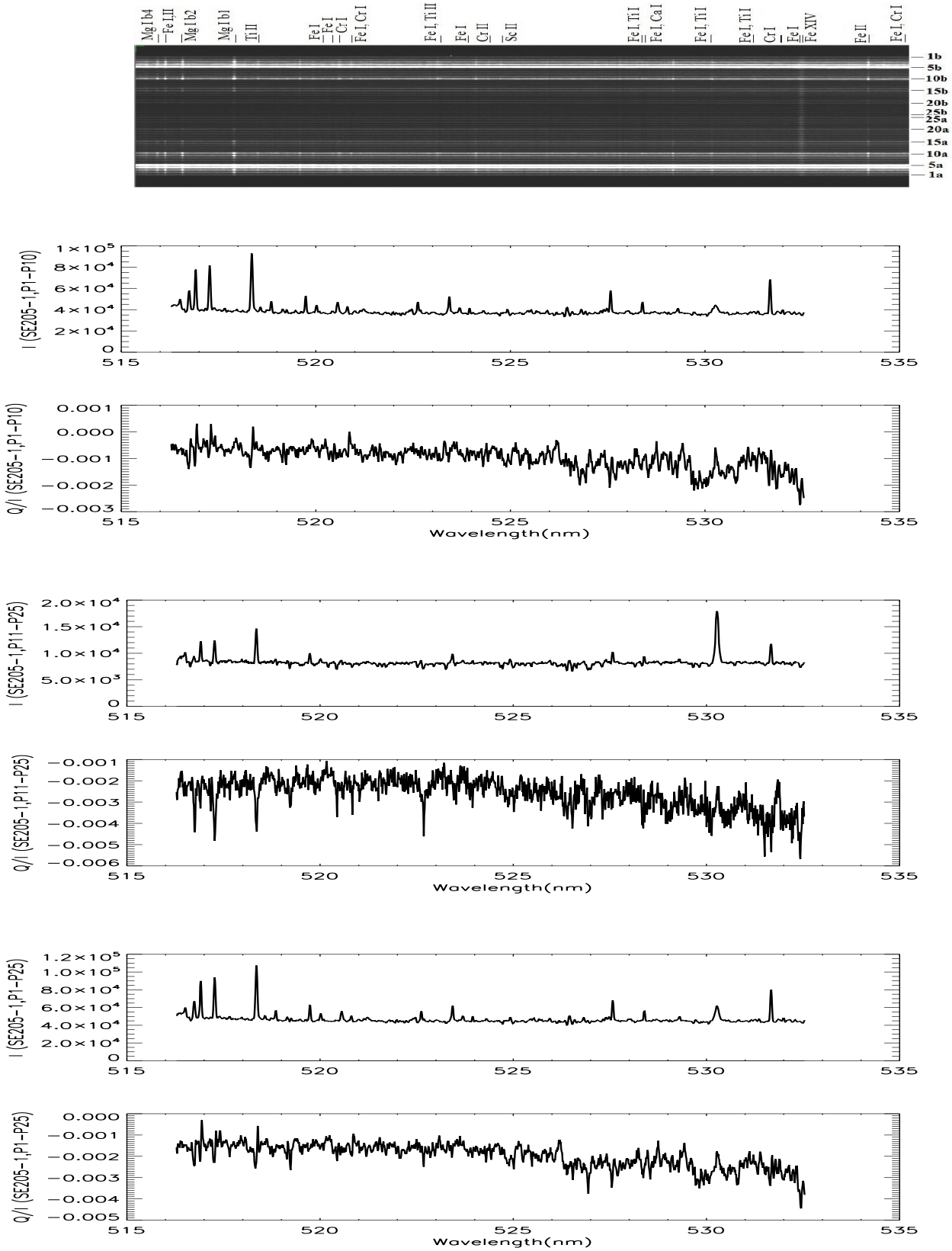

Fig. 6.— SE205-1. Top panel: the raw spectral image. Lower panels: the intensity I and fractional linear polarization Q/I profiles obtained in the panels below from the polarization demodulation after spatial binning over P1-P10, P11-P25 and all the volumes(P1-P25) of the FOV respectively. Note that the polarizations are given of F-corona, E-corona and K-corona.

FeI/CrI532.4nm line remains remarkable due to its polarization rather than its poor line depth. Many Fraunhofer lines have moderate polarization amplitudes, like these at 519.2nm, 526.9nm, 527.0nm, 530.1nm and 531.5nm. Again, some Fraunhofer lines, like those at 522.5nm, 523.2nm and 529.7nm, have no detectable polarization under the present polarimetric sensitivity of about 6.0×10^{-4}. Finally, amplitudes of the continuum polarization become larger from the shortest wavelength to the largest one by an increase of 0.18%, but they are smaller than those of most emission lines and most Fraunhofer lines. In other words, the F-corona and E-corona can be polarized more strongly than the K-corona.

The I and Q/I profiles of the whole FOV are respectively depicted in two bottom panels of Fig.6. The intensity profiles are closest to these of SE196-4 again, except the presence of the coronal line. But the Q/I profiles look differently from the other cases. Although more contribution comes from the lower layers to to the intensity as a result of the combination of the two divided regions, contribution of negative value of the polarization from the upper layers cannot be ignored. In fact, all the polarizations are integrated to be negative or parallel to the local solar limb. For FeI520.8nm, its totally combined Q/I takes a shape approximately antisymmetric about the line center, the lobe in the blue wing comes from the upper layers and the red wing lobe is contributed from the lower layers. The largest Q/I amplitude of about 0.18% is gained again by the Fraunhofer FeI/CrI 532.4nm line again. The polarization of the coronal line can be easily seen but that of the transition zone FeII531.7nm lines is almost merged in the noise.

From the above analysis, it becomes evident that some Fraunhofer lines such as the quartet, CrI/FeI520.8nm, FeI/TiII522.7nm, FeI523.3nm, and FeI/CrI532.4nm are much more easily polarized than other lines like FeI523.0nm, FeI/CrI524.7nm and FeI525.0nm. Furthermore, we have witnessed the great intensity variations of the same lines in different spatial points. They can be strong Fraunhofer lines in one spatial point, but hard to be recognizable in another, such as MgIb_4, FeI528.2nm, FeI/TiI528.3nm, and FeI528.8nm. Evidently, this phenomenon cannot be explained via scattering by dust in the F-corona.

3. Presence of neutral atoms in the inner corona

The above-mentioned properties of the Fraunhofer lines in the upper solar atmosphere revealed from the polarimetry make us search for the essence of the inner F-corona. It becomes clear that it cannot be dominantly originated from the dust scattering that should result in the maintenance of the relative intensities among the Fraunhofer lines as in the photosphere and the close linear polarimetric properties for different lines. In fact, even the relative intensities among these Fraunhofer lines in the inner corona are observed to be varied greatly from their photospheric counterparts. For instance, in the spectrum of the quartet in the upper layers(P11-P25) of the

FOV shown in Fig.5, their relative intensities of the spectral lines are greatly changed from their photospheric origins, and so do these Fraunhofer lines within sub-band from 520.0nm to 520.1nm.

Taking SE204-3 for example, the polarizations of the Fraunhofer lines differs so greatly that they can neither be ascribed to the dust scattering, since they depend on the wavelength or specific spectral lines as shown previously. Especially, the co-existence of Q/I profiles of the approximately antisymmetric shapes with one-peaked or one-valleyed Q/I profiles of the different Fraunhofer lines at the same point, further demonstrate that they cannot be deduced from the line-of-sight integration of the dust scattering. On the other hand, there are no critical changes of Q/I amplitudes of Fraunhofer lines, say, FeI532.4nm, from cases without the coronal line to those with the coronal line. Furthermore, variation of the Q/I profile of, say, MgIb_1 line, from the emission(in the lower layers) to the absorption appearance(in the upper layers) is essentially same as that of Fraunhofer line keeping their line depression appearance in the whole FOV, such as FeI520.8nm. All these incline to a conclusion that these Fraunhofer lines form in the inner corona with small amplitudes of linear polarization, or the amplitudes will be much greater(Blackwell,1956) beyond the inner corona since the scattering becomes more anisotropic with height;

The relative motions can provide further demonstration between two spatial volumes of these particles yielding the Fraunhofer lines revealed from the spectra in SE204-3 in the upper layers, derived from the relative shifts of line center wavelengths along the line-of-sight due to the Doppler effect.

In order to get the reliable polarimetric result, we have to perform binning over at least ten spatial points or two rows in the FOV. However, for purpose of the relative line-of-sight motion derivation, intensity profile of each spatial point, like these depicted in Fig.7, can be used from SE204-3, since the standard deviation of the noise fluctuation reads as 7cts, and the intensity differences between the line center and its closest wavelength samples are generally greater than the fluctuation. The relative motions indicated by Doppler shifts can be reflected in the wavelength distances between their line centers of these chosen Fraunhofer lines. The intensity profiles of four sample points P14, P16, P20 and P22 of SE204-3 in the inner corona are plotted in Fig.7. The center wavelengths of selected lines are listed in Tab.1 for data analysis.

It is easily seen from Tab.1 that the line center shifts vary for different lines. For instance, at MgI516.7nm under the present spectral resolution of 0.012nm, the wavelength displacement of the line centers between P20 and P22 becomes the greatest as 0.024nm, the same shift is found at FeI523.3nm, but only 0.012nm for FeI520.2nm and FeI/CrI520.8nm while no displacement at FeI/CrI532.4nm but opposite displacement for FeI/TiII522.7nm are found. On the other hand, the greatest displacement 0.024nm occurs between P14 and P16 for FeI/CrI532.4nm, but opposite displacement 0.012nm for MgI516.7nm and FeI522.7nm is revealed, while no displacement occurs for FeI520.2nm, 520.8nm and 523.3nm. Other similar non-synchronous displacements can be

found in this table. All of these specify that the Fraunhofer lines are not produced mainly from the dust scattering but individual atoms. These atoms are not confined in the dust but separately move as individually.

4. Discussion and Conclusion

In this paper, we present the spectropolarimetry of the Fraunhofer lines in upper solar atmosphere below elongation of about 0.04 solar radius including those forming in atom-induced F-corona during a solar eclipse. Four samples are given with different distribution style of particles yielding the Fraunhofer lines in the upper chromosphere, transition zone as well as the inner corona. Here are the summaries describing the polarimetric results:

1) The polarizations of the Fraunhofer lines and their adjacent continua can be easily distinguished in the spectropolarimetry. It becomes evident in cases shown in subsection 2.2 in the upper layers that the polarization amplitudes of both the E-corona and F-corona are generally greater than those of the continuum (K-corona) polarization in the inner corona. And it is evident that those Fraunhofer lines appeared with the green coronal line have polarization properties of amplitudes and orientations very close to those without the coronal lines. This may indicate their common photospheric origin for these Fraunhofer lines;

2) The polarizations of the Fraunhofer lines described by Q/I vary with space especially with elongation, in both the polarization amplitude and orientation. Higher the elongation is, greater the polarization amplitude is wrt the continuum polarization level as an overall trend. The distributions of polarizations of all these Fraunhofer lines are far from the homogeneity or symmetry in the inner solar corona;

3) The fractional linear polarizations of the Fraunhofer lines in these layers can reach a few thousandth. A greatest amplitude of about 0.36% is detected for the neutral magnesium b_1 Fraun-

Table 1: Line center positions of sample spectral lines in upper layers of SE204-3 (wavelengths in the table are in unit of nanometer)

	MgI516.7nm	FeI520.2nm	FeI/CrI520.8nm	FeI/TiII522.7nm	FeI523.3nm	FeI/CrI532.4nm
P14	516.760	520.207	520.826	522.671	523.266	532.429
P16	516.748	520.207	520.826	522.659	523.266	532.453
P20	516.736	520.195	520.814	522.683	523.254	532.441
P22	516.760	520.207	520.826	522.671	523.278	532.441

hofer line in case of SE204-3 after binning over the three higher rows of the FOV. This is basically consistent with the prediction by van de Hulst(1950) and observation by Blackwell(1956). They are often comparable with those of emission lines within the same FOVs;

4) Different Fraunhofer lines have generally different amplitudes even in the same volume and their Q/I profiles are structured. This means that the polarization is wavelength-dependent. There are some Fraunhofer lines which are more polarization-sensitive, such as MgI$b_{1,2}$, FeI/CrI532.4nm, than other lines like FeI525.0nm. This strongly suggests that the polarizations cannot be primarily ascribed to scattering by dust. Furthermore, the fractional linear polarization has nothing to do with the line intensity. Otherwise, spectral resolution becomes crucial especially to show the approximately antisymmetric Q/I profiles. In such a case, polarimetry with lower spectral resolution will result in the underestimation of the polarization amplitudes and lose the detail of the polarization feature of a specific line;

5) The linear polarization orientation can be changed and the change process can be accompanied by the Q/I profile configuration variation. In lower layers of all the cases containing the Fraunhofer lines, the fractional linear polarization of the Fraunhofer lines take a form of approximately antisymmetric shapes and then such an appearance turns to a configuration with amplitudes either above the continuum polarization level or below it. Another profile variation signifying the polarization orientation change is that positive Q/I amplitudes in the lower layers turn to be negative amplitudes in higher layers;

6) The continuum polarization becomes also greater with height. It has 0.05% or smaller percent polarization amplitude very close to the limb and can reach 0.30% in the higher layers. And sometimes it varies with wavelength, but the variation is not considerable. However, these amplitudes are generally smaller than those of emission or Fraunhofer lines.

All of these indicate that the mechanisms responsible for the emanation of linear polarization are very complex, due to anisotropic scattering among which atomic polarization may be a main factor leading to spectral line-dependent polarization(Landi Degl'Innocenti et al., 1983; Stenflo et al., 1997; Trujillo Bueno, 2002). These polarization properties revealed here can help us understand the physical contents of the outer solar atmosphere further. For instance, as a byproduct, the polarimetric property such as strong line-dependence and special Q/I profiles, along with other above-mentioned evidences, leads us to show the existence of neutral atoms in the inner corona, where the dust will be sublimated due to the high energy flux(Boe et al.,2021). Therefore, the inner F-corona described in this paper is actually induced by the neutral atoms of metals like iron, magnesium and chromium.

The presence of the neutral atoms like magnesium, iron and chromium indicates more microstates found in the inner corona than in those layers below. Thus it means an increase in entropy

from the photosphere to the corona, and it proves further that the corona is an open but multithermal system. Though contribution from other sources cannot be excluded like leakage from the magnetically confined type II spicules and the prominences, SE196-2, SE196-4 and many similar samples imply that these neutral atoms may originate dominantly from the photosphere with their profiles modified by the emission, absorption and Rayleigh scattering along the line-of-sight accompanying the upflows(Tian,2021). They escape from heating through chromosphere and transition zone. This extends the space of the cool matter, such as carbon monoxide molecules discovered in the chromosphere by Solanki and his cooperators(Solanki,1994). All of these establish a constraint on the chromospheric and coronal heating mechanisms.

This work is sponsored by National Science Foundation of China (NSFC) under the grant numbers 11078005, U1931206

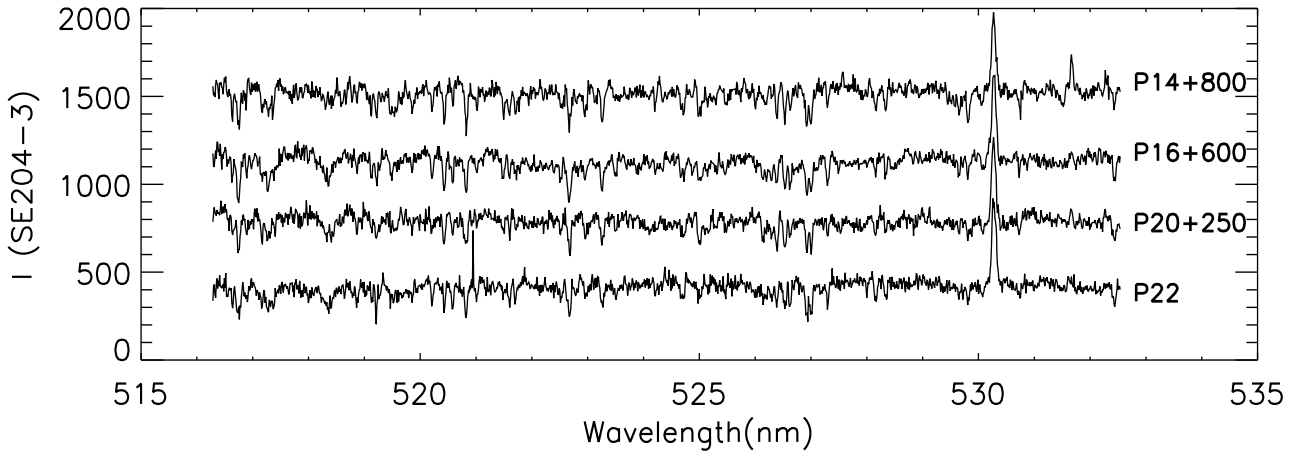

Fig. 7.— The intensity *I* profiles respectively of P14, P16, P20 and P22 of SE204-3 for illustrating the relative line center shifts due to Doppler effect. Note that a cosmic event causing a strong emission at 520.9nm at P22. The intensities of P20 are artificially added with 250cts, and intensities of both P16 and P14 are added respectively with 600cts and 800cts in order to separate these four profiles within one panel.

REFERENCES

Aschwanden, M.J., 2015, *Physics of the solar corona*. Springer, Published in association with Praxis Publishing Chichester, UK, ISBN: 3-540-22321-5

Bianda, M., Solanki, S. K., and Stenflo, J. O., Hanle depolarization in the solar chromosphere, A&A, 331, 760(1998)

Blackwell, D.E., 1956, *Mon. Not. R. Astron. Soc.* **116**,56

lackwell, D.E. and Petford, A.D., 1966, *Mon. Not. R. Astron. Soc.* **131**,399

Brueckner, G.E., Howard, R.A., Kooman, M.J., et al., 1995, *Sol.Phys.*, **162**, 357

Burtovoi, A. Naletto, G., Dolei, S., Spadaro, D., Romoli, M., F. Landini, F., and De Leo, Y., 2022, *Astron. & Astrophys.* **659**, A50

Boe, B., Habbal, S., Downs, C. and Druckmüller, M., 2021, *Astrophys. J.*, **912**, 44

Domingo, V., Fleck, B., and Poland, A.I., 1995, *Sol. Phys.*, **162**, 1

Gandofer, A., 2000, *The second Solar Spectrum, A High Spectral Resolution Polarimetric Survey of Scattering Polarization at the Solar Limb in Graphical Representation*. Vol. I: 4625Å to 6995 Å(*Zurich: vdf Hochschulverlag*), ISBN 3 7281 2764 7

Golub, L., Pasachoff, J.M., 1997, *The solar corona. Combridge University Press*, ISBN: 3-540-22321-5

Grotrian, Von W., 1934, *Zeitschrift für Astrophysik*. **8**,124

Grotrian, W., 1956, Polaritaeten und Maximalwerte magnetischer Feldstaerken von Sonnenflecken in den Jahren 1952-1953, *Publikationen des Astrophysikalischen Observatoriums zu Potsdam*, 1

Howard, R. A., Vourlidas, A., Bothmer, V., et al., 2019, *Nature*, **576**, 232

van de Hulst, H.C., 1950, *Bulletin of the Astronomical Institutes of the Netherlands*. **11**, 135

Koutchmy, S., and Magnant, F., 1973, *Astrophys. J.*, **186**, 671

Koutchmy, S., Baudin, F., Abdi, Sh. et al., 2019, *Astron. & Astrophys.*, **632**, A86

Lamy, P.L. et al., 1992, *Science* **257**, 1377-1380

Lamy, P.L., Gilardy, H., and LIebaria, A., 2022, *Space Sci. Rev.*, **218**, 53

Landi Degl'Innocenti, E., 1983, *Solar Phys.* **85**, 3

Lietzow, M., and Wolf, S., 2023, *Astron. & Astrophys.* **671**, 113

Minnaert, M., 1930, *Zeitschrift für Astrophysik*.**1**,209

Moore, J.H., 1934, *Publ. Astron. Soc. Pacific* **46**,298

Ohman, Y., 1947, Results from observation of the total solar eclipse of 1945 July 9:1. The polarization of the corona, *Stockholms Observatoriums Annular*, 15, No.2, 1

Qu, Z.Q., 2011, *ASPC Conf. Series*, 437, 423;

Qu, Z.Q. L. Chang, X.M. Cheng, et al., 2014, *ASPC Conf. Series*, 489, 263;

Qu, Z.Q., Dun, G.T., Chang, L. et al.,2017, *Solar Phys.*, 292, 37;

Qu, Z.Q., Chang, L., Dun, G.T., et al., 2022, *ApJ*, 940, 150;

Schuster, A., 1879,*Mon. Not. R. Astron. Soc.* **40**,35

Solanki, S.K., Livingston, W., and Ayres, T., *Science*, **263(5143)**, 64-66(1994)

Stenflo, J.O. and Keller, C.U., 1997,*Astron. & Astrophys*. **321**, 927

Tian, Hui, et al., *Sol. Phys.*, **296**, 47(2021)

Trujillo Bueno, J., Landi Degl'Innocenti, E., Collados, M., Merenda, L. and Manso Sainz, R., 2002, *Nature*, **415**, 403